Systematic Investigation of Nanoscale Adsorbate Effects at Organic Light-Emitting Diode Interfaces. Interfacial Structure−Charge Injection−Luminance Relationships

Qinglan Huang,[†,‡] Jianfeng Li,[†] Guennadi A. Evmenenko,[§] Pulak Dutta,[§] and Tobin J. Marks*[,†]

Departments of Chemistry and Physics and Astronomy and the Materials Research Center, Northwestern University, Evanston, Illinois 60208

Received February 28, 2006

Molecule-scale structure effects at indium tin oxide (ITO) anode−hole transport layer (HTL) interfaces in organic light-emitting diode (OLED) heterostructures are systematically probed via a self-assembly approach. A series of ITO anode-linked silyltriarylamine precursors differing in aryl group and linker density are synthesized for this purpose and used to probe the relationship between nanoscale interfacial chemical structure and charge-injection/electroluminescence properties. These precursors form conformal and largely pinhole-free self-assembled monolayers (SAMs) on the ITO anode surface with angstrom-level thickness control. Deposition of a HTL on top of the SAMs places the probe molecules precisely at the anode−HTL interface. OLEDs containing ITO/SAM/HTL configurations have dramatically varied hole-injection magnitudes and OLED responses. These can be correlated with the probe molecular structures and electrochemically derived heterogeneous electron-transfer rates for such triarylamine fragments. The large observed interfacial molecular structure effects offer an approach to tuning OLED hole-injection flux over 1−2 orders of magnitude, resulting in up to 3-fold variations in OLED brightness at identical bias and up to a 2 V driving voltage reduction at identical brightness. Very bright and efficient (∼70 000 cd/m^2, ∼2.5% forward external quantum efficiency, ∼11 lm/W power efficiency) Alq (tris-(8-hydroxyquinolinato)aluminum(III))-based OLEDs can thereby be fabricated.

Introduction

In the ongoing quest for high-performance organic solid-state optoelectronic devices, controlling organic−inorganic and organic−metal interfacial phenomena is thought to be vital to optimizing response properties by maximizing organic molecule−electrode physical/electrical contact and sustaining efficient charge injection.[1−4] Nevertheless, many nanoscale interfacial phenomena are frequently intermingled with bulk properties, requiring painstaking experimental efforts to identify genuinely interfacial characteristics. Currently, most interfacial analyses have largely relied on surface analytical methods such as the Kelvin probe,[5,6] photoelectron emission spectroscopy (e.g., ultraviolet photoelectron spectroscopy (UPS), X-ray photoelectron spectroscopy (XPS)), and scanning probe microscopy (AFM, STM).[7−13] Maintaining noncontaminated interface regions is critical to successful analysis, but it is not always achieved.

Interfacial effects on OLED electroluminance (EL) have been described from the point of view of charge injection,[14−16] energy-level matching,[17−19] physical delamination/decohe-

* To whom correspondence should be addressed. E-mail: t-marks@northwestern.edu.

† Department of Chemistry and the Materials Research Center, Northwestern University.

‡ Current address: GE Global Research, 1 Research Circle, Niskayuna, NY 12309.

§ Department of Physics and Astronomy and the Materials Research Center, Northwestern University.

(1) Koller, G.; Blyth, R. I. R.; Sardar, S. A.; Netzer, F. P.; Ramsey, M. G. *Appl. Phys. Lett.* **2000**, *76*, 927−929.
(2) Vuillaume, D.; Lenfant, S. *Microelectron. Eng.* **2003**, *70*, 539−550.
(3) Blyth, R. I. R.; Duschek, R.; Koller, G.; Netzer, F. P.; Ramsey, M. G. *J. Appl. Phys.* **2001**, *90*, 270−275.
(4) Ahles, M.; Schmechel, R.; von Seggern, H. *Appl. Phys. Lett.* **2004**, *85*, 4499−4501.
(5) Appleyard, S. F. J.; Day, S. R.; Pickford, R. D.; Willis, M. R. *J. Mater. Chem.* **2000**, *10*, 169−173.
(6) Zuppiroli, L.; Si-Ahmed, L.; Kamars, K.; Nüesch, F.; Bussac, M. N.; Ades, D.; Siove, A.; Moons, E.; Grätzel, M. *Eur. Phys. J. B* **1999**, *11*, 505−512.
(7) Forsythe, E.; Gao, Y. In *Handbook of Surfaces and Interfaces of Materials*; Nalwa, H. S., Ed.; Academic Press: London, 2001; Vol. 1, pp 285−327.
(8) Donley, C.; Dunphy, D.; Paine, D.; Carter, C.; Nebesny, K.; Lee, P.; Alloway, D.; Armstrong, N. R. *Langmuir* **2002**, *18*, 450−457.
(9) Goncalves-Conto, S.; Carrard, M.; Si-Ahmed, L.; Zuppiroli, L. *Adv. Mater.* **1999**, *11*, 112.
(10) Hill, I. G.; Gajagopal, A.; Kahn, A.; Hu, Y. *Appl. Phys. Lett.* **1998**, *73*, 662.
(11) Ishii, H.; Sugiyama, K.; Ito, E.; Seki, K. *Adv. Mater.* **1999**, *11*, 605−625.
(12) Nalwa, H. S. In *Handbook of Surfaces and Interfaces of Materials*; Nalwa, H. S., Ed.; Academic Press: London, 2001; Vol. 1.
(13) Schlaf, R.; Parkinson, B. A.; Lee, P. A.; Nebesny, K. W.; Armstrong, N. R. *Appl. Phys. Lett.* **1998**, *73*, 1026.
(14) Malinsky, J. E.; Veinot, J. C. G.; Jabbour, G. E.; Shaheen, S. E.; Anderson, J. D.; Lee, P.; Richter, A. G.; Burin, A. L.; Ratner, M. A.; Marks, T. J.; Armstrong, N. R.; Kippelen, B.; Dutta, P.; Peyghambarian, N. *Chem. Mater.* **2002**, *14*, 3054−3065.
(15) Nüesch, F.; Forsythe, E. W.; Le, Q. T.; Gao, Y.; Rothberg, L. J. *J. Appl. Phys.* **2000**, *87*, 7973.
(16) Appleyard, S. F. J.; Day, S. R.; Pickford, R. D.; Willis, M. R. *J. Mater. Chem.* **2000**, *10*, 169−173.
(17) Ganzorig, C.; Kwak, K. J.; Yagi, K.; Fujihira, M. *Appl. Phys. Lett.* **2001**, *79*, 272−274.
(18) Gross, M.; Müller, D.; Nothofer, H.; Scherf, U.; Neher, D.; Brauchle, C.; Meerholz, K. *Nature* **2000**, *405*, 661−665.
(19) VanSlyke, S. A.; Chen, C. H.; Tang, C. W. *Appl. Phys. Lett.* **1996**, *69*, 2160.

10.1021/cm0604918 CCC: $33.50
Published on Web 04/07/2006

Scheme 1. Scheme for ITO Surface Modification by Covalently Chemisorbed HTL Materials

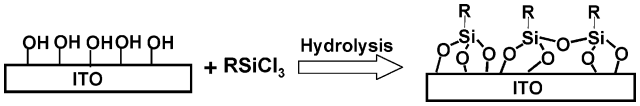

sion,[20,21] anode corrosion/ion injection,[22,23] interfacial dipoles,[11,24] image forces,[25] and exciton quenching.[26,27] As an example, diverse explanations for the effects of ITO anode−HTL interlayers have been proposed, including increased hole injection due to interface dipoles,[16] reduced injected charge backscattering,[28] reduced anode work function−HTL HOMO energetic barriers,[29] increased recombination efficiency by balancing electron and hole injection,[30,31] and/or confining electrons to the emissive layer.[32] Surface-energy-promoted wetting/cohesion at the indium tin oxide (ITO)−organic layer interface also plays a significant role.[33−35] Note that in the vast majority of these cases, systematic effects of anode−HTL interfacial molecular structure on OLED response have been largely left unexplored, reflecting the lack of suitable series of architecturally varied probe structures.

Previously, we communicated significant interfacial structure effects on OLED EL response via depositing conformal, robust, nanoscale self-assembled monolayers (SAMs) on ITO surfaces (Schemes 1 and 2).[36] As an extension of that preliminary work, we present here a systematic investigation of a series of interfacial probe molecules designed to specifically modify the OLED ITO anode−HTL interface. In this paper, we validate the argument that probe molecules can be precisely delivered to these interfacial regions, as evidenced by XPS, X-ray reflectivity, and electrochemistry measurements. Furthermore, we demonstrate that the present SAM−ITO anode approach is well-suited for electrochemical interrogation. Strong correlations are observed between electrochemical electron-transfer rates and charge-injection fluences across the SAMs at the ITO anode−electrolyte or HTL interface; these can be explained with classical heterogeneous electron-transfer theory, which affords a unique and practical method of measuring interfacial charge injection in OLEDs. Most importantly, we report for the first time that the large interfacial structure effects are predominantly responsible for the dramatic charge-injection variations seen here. Combined with the findings communicated previously,[36] our results provide a simple and effective route for selectively modifying ITO anode−HTL interfaces, with much less bulk-property interference than with traditional methods. Also, the rationally designed probe structures allow for in-depth study of interfacial structure effects on the OLED EL response, by tuning probe molecular structure/denticity, intermolecular interactions, and probe π-system−ITO anode spacing. Applying the above finding to tuning ITO−anode hole-injection flux results in up to three times the variation in OLED brightness at identical bias and up to a 2 V driving voltage reduction at identical device brightness. The interfacial hole-injection tuning leads to very bright and efficient ($\sim$70 000 cd/m^2, $\sim$2.5% external forward quantum efficiency, 11 lm/W power efficiency) Alq (tris (8-hydroxyquinolinato)aluminum(III))-based OLEDs that are $\sim$10 times brighter than devices lacking the interfacial tuning.

Experimental Section

Materials and Methods. ITO glass sheets (20 Ω/□, rms roughness = 2.5 nm) were purchased from Colorado Concept Coating. All chemical reagents were used as received unless otherwise indicated. All manipulations of air/moisture-sensitive materials were carried out on a dual-manifold Schlenk line or in a nitrogen-filled glovebox. Ether and THF were distilled from sodium/benzophenone ketyl. Methylene chloride was distilled from calcium hydride. Toluene was dried using activated alumina and Q5 columns and was regularly tested with benzyphenone ketyl in ether solution. Alq was purchased from Sigma-Aldrich and purified via vacuum gradient sublimation. The OLED component, 2,9-dimethyl-4,7-diphenyl-1,10-phenanthroline (BCP, Scheme 3), was purchased from Fluka and purified via vacuum gradient sublimation. The hole-transport material 1,4-bis(1-naphthylphenylamino)biphenyl (NPB) was synthesized according to the literature[37] and purified by recrystallization, followed by vacuum gradient sublimation. The fluorescent dopant *N*,*N*′-di(3-heptyl)quinacridone (DIQA, Scheme 3) was synthesized and purified according to the literature.[38] All other reagents were purchased from Sigma-Aldrich and used as received. The synthetic pathways to TPD-Si$_4$ and TAA-Si$_1$ are reported in the Supporting Information. The synthesis of TPD-Si$_2$ and TAA-Si$_3$ are reported elsewhere.[20] NMR spectra were obtained on Varian VXR-400 or 500 MHz NMR instruments, and MS analyses were conducted on a Micromass Quattro II Triple Quadrupole HPLC/MS/MS mass spectrometer. Elemental analyses were carried out by Midwest Microlab. UV−visible absorption spectra of SAM-coated quartz plates were obtained on a Cary 1E UV−vis spectrometer. Cyclic voltammetry was performed with a

(20) Cui, J.; Huang, Q.; Veinot, J. C. G.; Yan, H.; Wang, Q.; Hutchison, G. R.; Richter, A. G.; Evmenenko, G.; Dutta, P.; Marks, T. J. *Langmuir* **2002**, *18*, 9958−9970.
(21) Yu, W.; Pei, J.; Cao, Y.; Huang, W. *J. Appl. Phys.* **2001**, *89*, 2343.
(22) Kim, J. S.; Ho, P. K. H.; Murphy, C. E.; Baynes, N.; Friend, R. H. *Adv. Mater.* **2002**, *14*, 206.
(23) Wong, K. W.; Yip, H. L.; Luo, Y.; Wong, K. Y.; Lau, W. M.; Low, K. H.; Chow, H. F.; Gao, Z. Q.; Yeung, W. L.; Chang, C. C. *Appl. Phys. Lett.* **2002**, *80*, 2788−2790.
(24) Huang, L. S.; Tang, C. W.; Mason, M. G. *Appl. Phys. Lett.* **1997**, *70*, 152.
(25) Tutis, E.; Bussac, M. N.; Zuppiroli, L. *Appl. Phys. Lett.* **1999**, *75*, 3880−3882.
(26) Burin, A. L.; Ratner, M. A. *J. Phys. Chem. A* **2000**, *104*, 4704−4710.
(27) Li, F.; Tang, H.; Anderegg, J.; Shinar, J. *Appl. Phys. Lett.* **1997**, *70*, 1233.
(28) Zuppiroli, L.; Si-Ahmed, L.; Kamars, K.; Nüesch, F.; Bussac, M. N.; Ades, D.; Siove, A.; Moons, E.; Grätzel, M. *Eur. Phys. J. B* **1999**, *11*, 505−512.
(29) Lee, S. T.; Wang, Y. M.; Hou, X. Y.; Tang, C. W. *Appl. Phys. Lett.* **1998**, *74*, 670.
(30) Malinsky, J. E.; Jabbour, G. E.; Shaheen, S. E.; Anderson, J. D.; Richter, A. G.; Marks, T. J.; Armstrong, N. R.; Kippelen, B.; Dutta, P.; Peyghambarian, N. *Adv. Mater.* **1999**, *11*, 227−231.
(31) Forsythe, E. W.; Abkowitz, M. A.; Gao, Y. *J. Phys. Chem. B* **2000**, *104*, 3948−3952.
(32) Ho, P. K. H.; Granstrom, M.; Friend, R. H.; Greenham, N. C. *Adv. Mater.* **1998**, *10*, 769.
(33) Cui, J.; Huang, Q.; Wang, Q.; Marks, T. J. *Langmuir* **2001**, *17*, 2051−2054.
(34) Cui, J.; Huang, Q.; Veinot, J. G. C.; Yan, H.; Marks, T. *Adv. Mater.* **2002**, *14*, 565.
(35) Xu, M. S.; Xu, J. B. *J. Phys. D: Appl. Phys.* **2004**, *37*, 1603−1608.
(36) Huang, Q.; Evmenenko, G.; Dutta, P.; Marks, T. J. *J. Am. Chem. Soc.* **2003**, *125*, 14704−14705.
(37) Koene, B. E.; Loy, D. E.; Thompson, M. E. *Chem. Mater.* **1998**, *10*, 2235−2250.
(38) Shaheen, S. E.; Kippelen, B.; Peyghambarian, N.; Wang, J. F.; Anderson, J. D.; Mash, E. A.; Lee, P. A.; Armstrong, N. R.; Kawabe, Y. *J. Appl. Phys.* **1999**, *85*, 7939−7945.

Scheme 2. Structures of Chlorosilane-Tethered Molecular Probes for Studying ITO Anode−HTL Interfacial Molecular Structure Effects on OLED Response

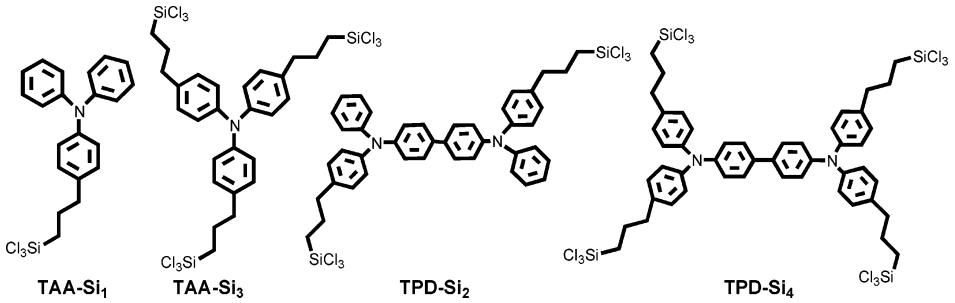

Scheme 3. Structures of Multilayer OLED Constituent Materials NPB (HTL), Alq (EML/ETL), DIQA (EML dopant), and BCP (ETL)

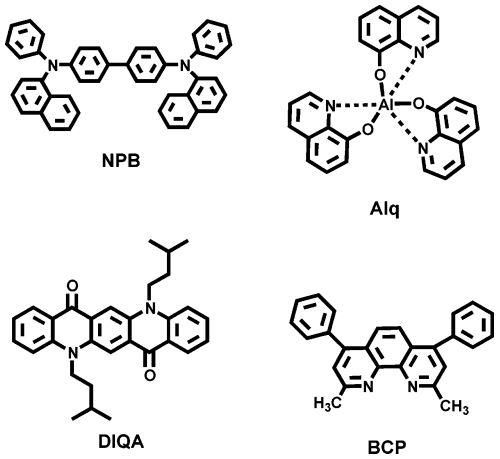

BAS 100 electrochemical workstation (SAM-coated ITO with ∼1 cm ^{2} area working electrodes, Ag wire pseudoreference electrode, Pt wire counter electrode, 0.1 M TBAHFP in anhydrous MeCN supporting electrolyte, and 1.0×10^{-3} M ferrocene as an internal pinhole probe. Scan rate = 0.1−10 V/s.). TBAHFP was recrystallized from an ethyl acetate/hexanes mixture and dried in vacuo at 100 °C for 10 h. Ferrocene was purchased from Sigma-Aldrich and purified via vacuum gradient sublimation. Specular X-ray reflectivity experiments on coated single-crystal Si (111) or Si (100) substrates were performed on the Naval Research Laboratory X23B beamline at the National Synchrotron Light Source. Data were acquired and analyzed as described previously.[39] XPS measurements were performed at Northwestern University with an Omicron ESCA probe, which was equipped with an EA125 energy analyzer. Photoemission was stimulated by monochromatic Al Kα radiation (1486.6 eV) with an operating power of 300 W, and a low-energy electron flood gun was employed for charge neutralization. Binding energies of spectra were referenced to the C 1s binding-energy set at 284.8 eV. UPS experiments on TPD-Si_2 and TAA-Si_3 SAM-coated ITO substrates were carried out at the University of Arizona using the 21.2 eV He(I) source (Omicron H15-13) of a Kratos Axis-165 Ultra photoelectron spectrometer. HOMO values were estimated from the median energy of the clearly defined photoionization peak, whereas IP values were estimated from the extrapolation of the high-kinetic-energy edge of that peak to zero intensity. The morphologies of all thin films were evaluated by atomic force microscopy (AFM) using a Nanoscope III microscope with A and D scanners (Digital Instruments, Inc.). All images were recorded under ambient conditions in the contact mode using Si_3N_4 cantilevers containing pyramidal tips with 70° cone angles and 20−50 nm radii of curvature. The cantilever had a force constant of 0.12 N/m. The images were obtained using the height mode with a total force of 20−60 nN and a scan rate of ∼10 Hz. The same image was scanned at least three times to ensure the reproducibility and was scanned at different area sizes (i.e., higher or lower magnifications) to verify image consistency. All the RMS surface roughness values are reported over an area of 25 μm^2. Advancing aqueous angles were measured on SAM-coated ITO substrates immediately after the self-assembly process.

Self-Assembly of Molecular Probes on ITO Substrates. ITO substrates were cleaned in an ultrasonic detergent bath, followed by methanol, 2-propanol, and finally acetone. The substrates were subsequently treated in an oxygen plasma cleaner for 1 min to remove any residual organic contaminants. Following strict Schlenk protocol, the clean ITO substrates were immersed in a 1.0 mM dry toluene solution of the silyltriarylamine molecules (Schemes 1 and 2). After being heated at ∼80 °C for 1 h, the toluene solution was decanted by cannula, and the substrates were rinsed with dry toluene (2 × 50 mL) and then wet acetone; the substrates were then transferred to a 120 °C oven for 1 h to expedite cross-linking.

Self-Assembly of the Molecular Probes on Silicon and Quartz Substrates. Quartz (Chemglass) or silicon (111) or (100) substrates (Semiconductor Processing Co.) were subjected to the following cleaning procedure: immersion in "piranha" solution (70:30 v/v concentrated H_2SO_4:30% H_2O_2) at 80 °C for 1 h. After being cooled to room temperature, substrates were rinsed repeatedly with deionized (DI) water, followed by an RCA-type cleaning protocol (5:1:1 v/v H_2O:30% H_2O_2:NH_3; sonication at room temperature for 40 min). The substrates were finally rinsed with copious amounts of DI water, heated to 125 °C for 15 min, and dried in vacuo. The molecular probes were then self-assembled onto the clean silicon substrates following the procedure described above for ITO substrates.

Fabrication of OLED Devices. The bare and SAM-coated ITO substrates were loaded into a bell jar deposition chamber housed in a nitrogen-filled double glovebox. A typical deposition procedure is as follows: At 1×10^{-6} Torr, a 20 nm layer of NPB was first deposited, followed by 60 nm of Alq doped with 1% DIQA. Both organic layers were grown at a deposition rate of 2−3 Å/s. Another 20 nm thick organic layer of BCP was then deposited, followed by thermal evaporation of a 1 nm thick Li layer. Finally, a 100 nm thick AgMg cathode was deposited through a shadow mask by coevaporating Ag and Mg in a 1:10 weight ratio. This metallic layer was patterned to afford four devices, each with an area of 0.10 cm^2. OLED device characterization was carried out with a computer-controlled Keithley 2400 source meter and an IL 1700 Research Radiometer equipped with a calibrated silicon photodetector at 25 °C under an ambient atmosphere. External forward quantum efficiencies were estimated from current density vs voltage and luminance vs current density characteristics.

(39) Cui, J.; Huang, Q.; Veinot, J. C. G.; Yan, H.; Wang, Q.; Hutchison, G. R.; Richter, A. G.; Evmenenko, G.; Dutta, P.; Marks, T. J. *Langmuir* **2002**, *18*, 9958−9970.

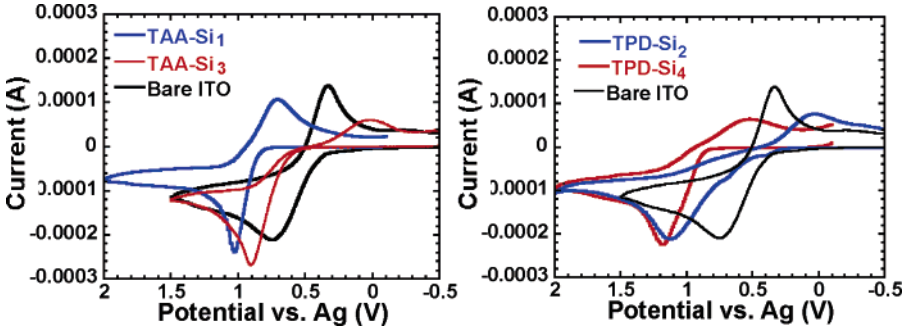

Figure 1. Cyclic voltammetry characteristics of self-assembled siloxane films on an ITO electrode immersed in a ferrocene solution. Coated ITO, silver wire, and Pt wire were used as the working, reference, and counter electrodes, respectively. All experiments were carried out in a 0.10 M acetonitrile solution of tetrabutylammonium hexafluorophosphate as the electrolyte and 0.0010 M ferrocene as the internal probe. Scan rate = 0.10 V/s.

Fabrication of Hole-Only Devices. Bare and SAM-coated ITO substrates were loaded into a bell jar deposition chamber housed within a nitrogen-filled double glovebox. At a base pressure of 1 $\times$ 10^{-6} Torr, NPB (400 nm) was vapor deposited at a rate of ~3 Å/s, followed by sputter-coating of a 6 nm Au layer through the same shadow mask employed for OLED fabrication described above. Single-carrier device assembly was subsequently completed with the masked thermal vapor deposition of Al (150 nm). The device behavior was evaluated using the above computer-controlled Keithley 2400 sourcemeter.

Results

We first discuss the chemisorptive deposition and subsequent characterization of self-assembled films of TAA-Si_1, TAA-Si_3, TPD-Si_2, and TPD-Si_4. These films are precisely located at the ITO anode−NPB HTL interface, and the relationship between the SAM molecular structure, electronic/electrochemical, and hole-injection efficiency can be probed. Finally, OLED response characteristics with these various structures at the ITO anode−NPB HTL interface are analyzed.

Deposition of the Molecular Probes onto ITO Substrates as well as onto Silicon and Quartz. The chlorosilane-tethered probe molecule series shown in Scheme 2 are self-assembled onto the hydrophilic ITO substrate surfaces with nanoprecise control in thickness, utilizing a self-limiting, solution-based chemisorption process. As illustrated in Scheme 1, clean ITO-coated glass surfaces possess hydroxyl functionalities and chemisorbed water that are reactive toward chlorosilanes, thereby achieving covalent binding of the silanes to the surface.[40] Further exposure to air and moisture in the following wet acetone rinse in air hydrolyzes any unreacted trichlorosilyl groups. Thermal curing facilitates the formation of cross-linked siloxane networks, resulting in a thin layer consisting of hole-transporting motifs covalently anchored to the ITO surface. At the completion of the silane condensation, chlorine concentrations in the film are below XPS detection limits.[8,14] Deposition of the probe molecules onto single-crystal Si or quartz substrates reasonably follows a similar chemisorption pathway. Thin-film characterizations are presented below.

Self-Assembled Siloxane Film Characterization. *Aqueous Contact Angle, UV−Visible Optical Absorption.* The surface energy of ITO glass substrates is changed dramatically upon arylamine thin-film deposition, as indicated by the large increases in advancing aqueous contact angles from ~20 (ITO) to ~90° (SAM/ITO). Also, these measurements indicate that the ITO substrates coated with the different SAMs have similar surface energies, as indexed by the nearly identical contact angles. The thin films deposited on quartz substrates were also analyzed by UV−visible optical absorption spectroscopy. The TAA-Si_3 and TAA-Si_1 films exhibit similar absorption characteristics (λ_{max} = 303 and 304 nm, respectively), as do films having TPD-Si_2 and TPD-Si_4 constituents (λ_{max} = 352 nm). The absorption maxima can be attributed to $n-\pi^*$ and $\pi-\pi^*$ optical excitations of the triarylamine cores.

Atomic Force Microscopy. AFM images of the self-assembled siloxane films on ITO substrates are essentially indistinguishable from the bare ITO substrate image with no indication of island growth, film cracking, or pitting. The rms roughnesses of bare ITO and TAA-Si_1, TAA-Si_3, TPD-Si_2, and TPD-Si_4 films on ITO were determined to be 2.56, 2.81, 2.67, 1.39, and 2.01 nm, respectively. This argues that the present self-assembly process is capable of depositing smooth, conformal siloxane films, with the TPD-Si_2 film providing some degree of ITO substrate planarization.

Pinhole Assessment by Ferrocene Cyclic Voltammetry. To further examine the present self-assembled siloxane films for pinholes over the entire ITO substrate area (1 cm^2), we carried out cyclic voltammetry experiments using ferrocene as a redox probe.[41] Here, the self-assembled siloxane-film-coated ITO substrates were used as working electrodes with bare ITO substrates used as references to calibrate the ferrocene redox potential for each measurement. The results are shown in Figure 1. The ferrocene oxidation peak potential is ~0.70 V with the bare ITO substrate as the working electrode and is shifted to 1.0 (TAA-Si_1), 0.90 (TAA-Si_3), 1.1 (TPD-Si_2), and 1.2 V (TPD-Si_4), respectively, with the self-assembled film-coated ITO substrates as working electrodes. The lack of significant current flow near the formal oxidation potential of ferrocene indicates an inhibition of ferrocene oxidation, resulting from conformal and largely pinhole-free film coverage of the ITO.[42,43] As the triarylamine oxidation potentials are reached, an electrocatalytic current

(40) Ulman, A. *Chem. Rev.* **1996**, *96*, 1533−1554.
(41) DuBois, C. J., Jr.; McCarley, R. L. *J. Electroanal. Chem.* **1998**, *454*, 99−105.
(42) Inzelt, G. In *Electroanalytical Chemistry*; Bard, A. J., Rubenstein, I., Eds.; Marcel Dekker: New York, 1994; Vol. 18, pp 90−134.
(43) Finklea, H. O. In *Electroanalytical Chemistry*; Bard, A. J., Rubenstein, I., Eds.; Marcel Dekker: New York, 1996; Vol. 19, pp 177−194.

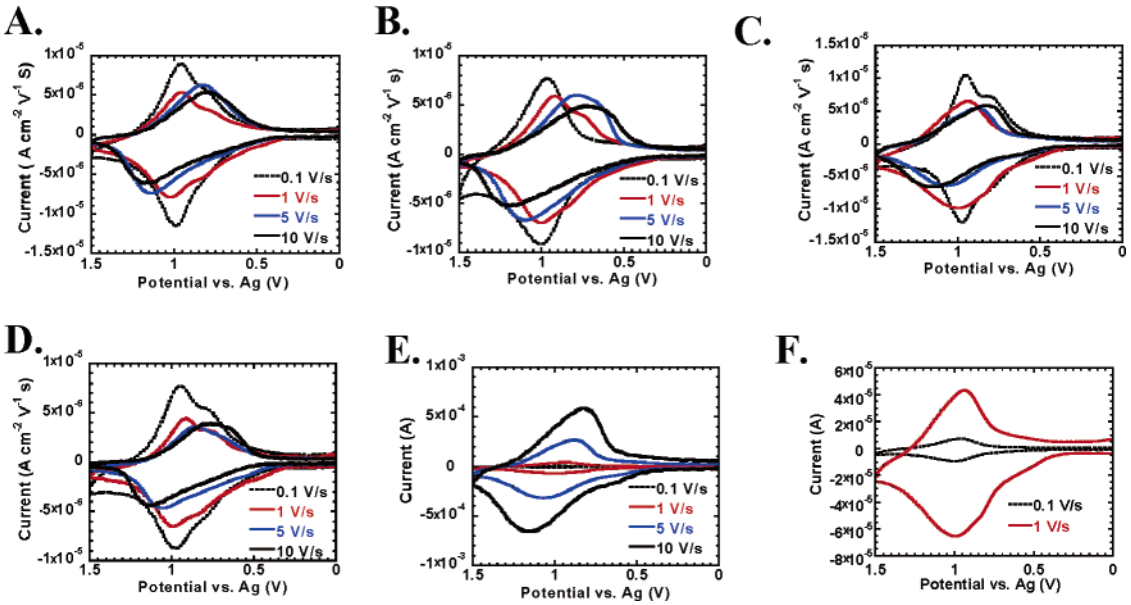

Figure 2. Cyclic voltammetry characteristics of self-assembled triarylamine siloxane films on ITO electrodes immersed in a 0.10 M acetonitrile solution of tetrabutylammonium hexafluorophosphate at scan rates of 0.1, 1.0, 5.0, and 10 V/s. Coated ITO, silver wire, and Pt wire were used as the working, reference, and counter electrodes, respectively. Currents are divided by the electrode area and scan rate to be normalized. (a) TAA-Si_1, (b) TAA-Si_3, (c) TPD-Si_2, and (d) TPD-Si_4. (e) Cyclic voltammetry characteristics of TAA-Si_1 with nonnormalized current; (f) those characteristics at scan rate 0.1 and 1 V/s expanded. Other siloxane-film-coated ITO electrodes exhibit similar nonnormalized current−voltage characteristics.

Table 1. Cyclic Voltammetry Characteristics of Self-Assembled Siloxane Films on an ITO Electrode Immersed in a Ferrocene Solution at Various Scan Rates[a]

	TAA-Si_1	TAA-Si_3	TPD-Si_2	TPD-Si_4
$E_{p,a}/E_{p,c}$ (V, scan rate 0.1 V/s)	0.987/0.960	1.004/0.970	0.970/0.945	0.975/0.954
$E_{p,a}/E_{p,c}$ (V, scan rate 1.0 V/s)	1.025/0.951	1.008/0.916	1.010/0.937	1.012/0.940
$E_{p,a}/E_{p,c}$ (V, scan rate 5.0 V/s)	1.142/0.825	1.104/0.779	1.067/0.875	1.063/0.854
$E_{p,a}/E_{p,c}$ (V, scan rate 10 V/s)	1.180/0.798	1.200/0.734	1.160/0.815	1.130/0.799
$\Delta E_{p,1/2}$ (V) [b]	0.340	0.460	0.350	0.440
coverage Γ ($\times 10^{-10}$ mol/cm^2)[b]	4.5	4.2	2.5	2.1
$E_{p,a} - E_{p,c}$ (V) [c]	0.382	0.466	0.345	0.331

[a] Coated ITO, silver wire, and Pt wire were used as the working, reference, and counter electrodes, respectively. [b] From cyclic voltammetry (0.1 V/s). [c] From cyclic voltammetry (10 V/s).

response is observed. This indicates that ferrocene is oxidized at an essentially diffusion-controlled rate,[44] meaning that facile triarylamine group oxidation at the ITO−HTL interface (hole injection) and rapid hole migration (presumably accompanied by counteranion migration) through the nanoscopic film occurs such that ferrocene oxidation takes place at the film−solution interface.

Redox Property Assessment by Cyclic Voltammetry. Electrochemical characteristics of the siloxane films were also investigated by cyclic voltammetry. In this case, the film-coated ITO substrates were used as the working electrode in a 0.1 M acetonitrile solution of tetrabutylammonium hexafluorophosphate as the electrolyte, but without the ferrocene. The sweep rate was varied from 0.1 to 10 V/s. The cyclic voltammetry curves obtained are shown in Figure 2. At a scan rate of 0.1 V/s, the oxidation/reduction line shape potentials are nearly symmetrical and almost identical for all of the SAM-coated electrodes, indicating that the rate of electron transfer is rapid on the time scale of the experiment.[45] As the scan rate is increased, redox peak potentials shift symmetrically in positive and negative directions, with broader peak shapes and greater separations between oxidation and reduction peak potentials indicating that the electron transfer is less reversible at more-rapid sweep rates.[46] Redox peak potentials ($E_{p,a}/E_{p,c}$) and maximum widths at half-height of the oxidation peak ($\Delta E_{p,a,1/2}$) are summarized in Table 1. Surface coverages of the triarylamine absorbates on ITO were estimated from integration of the oxidation peak areas (eq 1). Here, Q is the total charge required for oxidation of the bound absorbate, n is the number of electrons required for oxidation of a single absorbate molecule, F is Faraday's constant, A is the total electrode area, and Γ is the surface coverage of the absorbates per unit electrode area.

$$Q = nFA\Gamma \tag{1}$$

UPS. UPS studies provide an estimate of the ionization potential and median HOMO energy for chemisorbed molecular systems.[11,47] HOMO values were estimated from the median energies of the clearly defined photoionization peaks, whereas IP values were estimated from the extrapolation of

(44) Liu, H. Y.; Yamamoto, H.; Wei, J. J.; Waldeck, D. H. *Langmuir* **2003**, *19*, 2378−2387.
(45) Chidsey, C. E. D.; Bertozzi, C. R.; Putvinski, T. M.; Mujsce, A. M. *J. Am. Chem. Soc.* **1990**, *112*, 4301−4306.
(46) Weber, K.; Creager, S. E. *Anal. Chem.* **1994**, *66*, 3164−3172.
(47) Anderson, J. D.; McDonald, E. M.; Lee, P. A.; Anderson, M. L.; Ritchie, E. L.; Hall, H. K.; Hopkins, T.; Mash, E. A.; Wang, J.; Padias, A.; Thayumanavan, S.; Barlow, S.; Marder, S. R.; Jabbour, G. E.; Shaheen, S.; Kippelen, B.; Peyghambarian, N.; Wightman, R. M.; Armstrong, N. R. *J. Am. Chem. Soc.* **1998**, *120*, 9646−9655.

Scheme 4. Energy-Level Diagram for the Electrodes and Organic Layers[a]

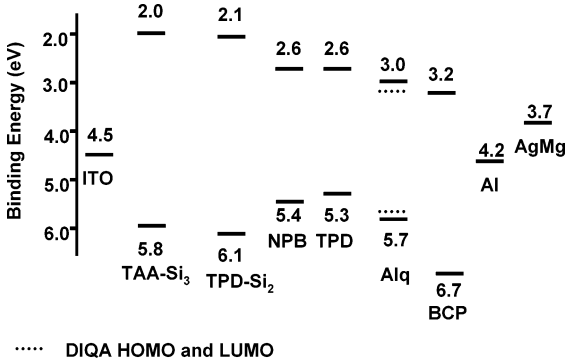

[a] Diagram taken from literature data.

Table 2. X-ray Reflectivity Characterization of Self-Assembled Triarylamine−Siloxane Layers on Single-Crystal Si (100) Substrates

	TAA-Si_1	TAA-Si_3	TPD-Si_2	TPD-Si_4
electron density (e Å^{-3})	0.31	0.32−0.34	0.32−0.35	0.30−0.33
roughness (Å)	3.9−4.0	7.5−7.6	7.4−8.2	12−14
thickness (Å)	10.9−11.1	13.4−13.6	17.7−17.9	16.1−16.3
foot print (Å^2)	44−50	51−66	51−58	80−98
calcd coverage Γ ($\times 10^{-10}$ mol/cm^2)	3.3−3.8	2.5−3.0	2.8−3.3	1.7−2.1

the high-kinetic-energy edge of the peak to zero intensity. The HOMO values for TAA-Si_3- and TPD-Si_2-coated ITO substrates are 5.8 and 6.1 eV, respectively, suggesting that the siloxane network of the self-assembled HTL does not drastically affect the electronic properties of the organic core structures and that the self-assembled siloxane films should support hole injection/transport in OLED devices (Scheme 4).

Specular X-ray Reflectivity (XRR). XRR measurements were performed on films deposited on clean, single-crystal Si(111) or Si (100) surfaces, using the self-assembly procedure described above. Fitting of the data to a physically reasonable model[48] provides details of the film thickness, smoothness, electron density, etc., as summarized in Table 2. Here, the surface coverages are calculated as follows: first, the film electron density per unit substrate area, N_{film}, is calculated using electron-density profiles obtained from the measurements. Then, the molecular footprint dimensions are calculated as N_{mol}/N_{film}, where N_{mol} is the calculated number of electrons in one molecular unit. Finally, surface coverages are derived by dividing the unit substrate area by the molecular footprint.

XPS. To confirm the proposed chlorosilane hydrolysis pathway depicted in Scheme 1, we performed XPS studies on self-assembled TPD-Si_4 thin films coated on ITO substrates. The results are shown in Figure 3. The characteristic signatures of Cl (2p) photoelectrons at 200 eV are below the detection limit, indicating completion of the silane hydrolysis/condensation. Also, a peak characteristic of Si (2p) at 102.9 eV is attributable to Si−O hydrolysis products.[14,49]

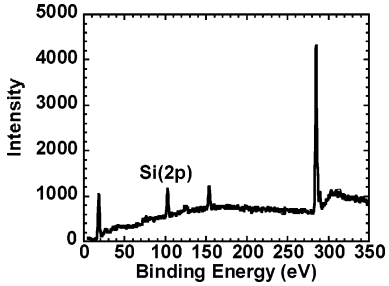

Figure 3. Representative X-ray photoelectron spectroscopy data showing the response from a self-assembled TPD-Si_4 film on an ITO substrate.

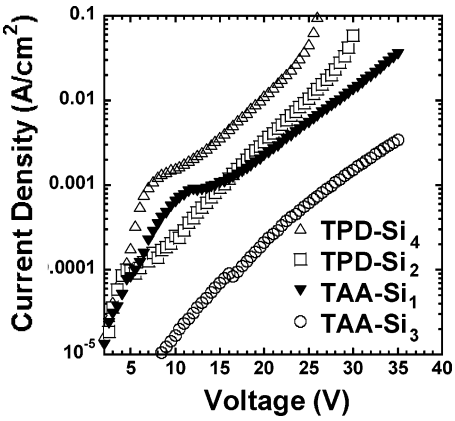

Figure 4. Effect of SAM structure on hole injection for hole-only devices with structures ITO/SAM/*N*,*N*-naphthyl-*N*,*N*′-phenyl-biphenyl-4,4′-diamine (NPB, 400 nm)/Au/Al.

Effects of the Self-Assembled Siloxane Films on Hole-Injection Efficiency. Hole-Only Devices. The effects of siloxane films incorporating various triarylamine probe molecules (Scheme 2) on ITO−organic interfacial hole injection were investigated by fabricating hole-only devices with structures of ITO/SAM/(NPB, 400 nm)/Au/Al.[50] Because of the high work function of gold (5.2 eV), electron injection from the Al cathode is largely blocked, so that hole currents dominate the charge transport in the above devices. The results are shown in Figure 4. Because the only difference in the four types of hole-only devices is in the self-assembled films, the results clearly reveal a significant structural sensitivity of hole injection across the nanointerfacial region. For example, hole current densities at 25 V are ~0.0004 A/cm^2 (TAA-Si_3) < ~0.004 A/cm^2 (TAA-Si_1) < ~0.01 A/cm^2 (TPD-Si_2) < ~0.04 A/cm^2 (TPD-Si_4); hole-injection fluences vary by 1−2 orders of magnitude.

Effects of the Self-Assembled Siloxane Interfacial Layers on OLED Response. OLEDs were next fabricated to examine the effects of the self-assembled siloxane films on EL response. Archetypical Alq-based OLEDs with structures of ITO/siloxane (1−2 nm)/NPB (20 nm)/Alq:1% DIQA (60 nm)/Al were studied first. Significant effects of the self-assembled films on luminance and efficiencies can be seen in Figure 5. Compared to ITO/NPB (20 nm)/Alq: 1% DIQA (60 nm)/Al OLEDs, OLEDs with the self-assembled films at the ITO anode−NPB HTL interface have greater current densities at identical bias. For instance, the current densities at 9 V are 0.12 A/cm^2 (TPD-Si_4) > 0.050

(48) Richter, A. G.; Yu, C. J.; Datta, A.; Kmetko, J.; Dutta, P. *Phys. Rev. E* **2000**, *61*, 607−615.
(49) Seah, M. P. In *Practical Surface Analysis: by Auger and X-ray Photoelectron Spectroscopy*; Briggs, D., Ed.; John Wiley & Sons: New York, 1983; Vol. 14, pp 181−254.
(50) Crone, B. K.; Campbell, I. H.; Davids, P. S.; Smith, D. L. *Appl. Phys. Lett.* **1998**, *73*, 3162−3164.

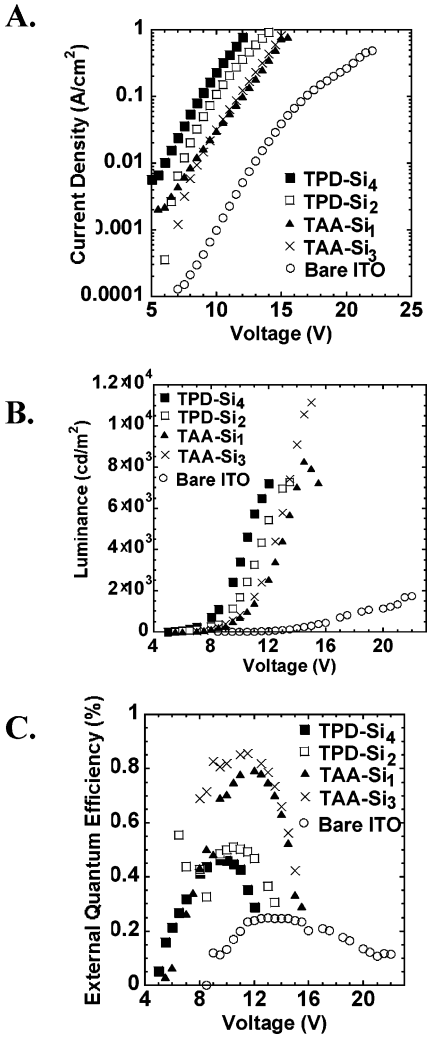

Figure 5. Responses of OLEDs with the structures ITO/SAM/NPB/Alq: 1% DIQA/Al. (a) Current density vs voltage; (v) luminance vs voltage; (c) external forward quantum efficiency vs voltage.

A/cm^2 (TPD-Si$_2$) > 0.016 A/cm^2 (TAA-Si$_1$) > 0.014 A/cm^2 (TAA-Si$_3$) > 0.00043 A/cm^2 (bare ITO), paralleling the same order of hole current densities measured above. Also, turn-on voltages are significantly reduced from 9 V for bare ITO-based OLEDs to 4−5 V for the self-assembled siloxane-film-based devices. This result indicates a substantial reduction of hole-injection barriers via ITO anode−NPB HTL interfacial modification. The maximum forward external quantum efficiencies are 0.25% (bare ITO) < 0.50% (TPD-Si$_4$) < 0.60% (TPD-Si$_2$) < 0.80% (TAA-Si$_1$) < 1.0% (TAA-Si$_3$). Luminances at 20 mA/cm^2 (a standard current density for device evaluation) are 168 cd/m^2 (bare ITO) < 200 cd/m^2 (TPD-Si$_4$) < 230 cd/m^2 (TPD-Si$_2$) < 400 cd/m^2 (TAA-Si$_1$) < 570 cd/m^2 (TAA-Si$_3$) (Figure 5).

In a second device configuration with an enhanced electron injection and a hole, exciton-blocking layer,[51,52] (ITO/siloxane (1−2 nm)/NPB (20 nm)/Alq:1% DIQA (60 nm)/BCP (20 nm)/Li (1 nm)/AgMg), strong self-assembled film nanostructure−OLED response correlations are again observed

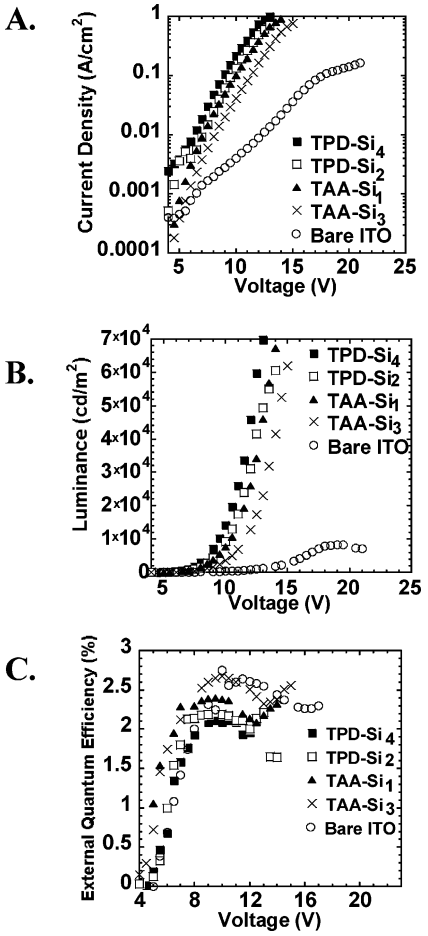

Figure 6. Responses of OLEDs with the structures ITO/SAM/NPB/Alq: 1% DIQA/2,9-BCP/Li/AgMg. (a) Current density vs voltage; (b) luminance vs voltage; (c) external forward quantum efficiency vs voltage.

(Figure 6). OLEDs with the self-assembled films at the ITO anode−NPB HTL interface again support greater current densities vs that of ITO/NPB (20 nm)/Alq:1% DIQA (60 nm)/BCP (20 nm)/Li (1 nm)/AgMg at identical bias. For instance, the current densities at 9.0 V are 0.11 A/cm^2 (TPD-Si$_4$) > 0.061 A/cm^2 (TPD-Si$_2$) > 0.049 A/cm^2 (TAA-Si$_1$) > 0.020 A/cm^2 (TAA-Si$_3$) > 0.0028 A/cm^2 (bare ITO). Light outputs vary significantly with different self-assembled siloxane film structures. For example, luminances at 9.0 V are ∼7000 cd/m^2 (TPD-Si$_4$) > ∼4200 cd/m^2 (TPD-Si$_2$) > ∼3700 cd/m^2 (TAA-Si$_1$) > ∼1600 cd/m^2 (TAA-Si$_3$) > ∼200 cd/m^2 (bare ITO), demonstrating the great capability of tuning hole injection and light output via modification of the ITO anode−HTL interface. Compared to ITO/siloxane/NPB/Alq:1% DIQA/Al OLEDs, the second device configuration yields superior device response, with the maximum luminance and forward external quantum efficiency achieved by TPD-Si$_4$-based OLEDs (∼70 000 cd/m^2 and 2.3%, respectively) nearly 1 order of magnitude and 5 times greater, respectively, than those values in Figure 5. This is attributable to the enhanced hole−electron density balance and more-efficient recombination via addition of the electron transporting/hole, exciton-blocking layer, BCP, and replacement of the Al cathode with AgMg.[52]

(51) Yang, C.-H.; Tai, C.-C.; Sun, I. W. *J. Mater. Chem.* **2004**, *14*, 947−950.
(52) Huang, Q. L.; Cui, J.; Veinot, J. G. C.; Yan, H.; Marks, T. J. *Appl. Phys. Lett.* **2003**, *82*, 331−333.

Discussion

Defining the Monolayer Deposition Process by Surface Coverage and Thickness. As schematically shown in Scheme 1, the trichlorosilane-tethered molecules (Scheme 2) form monolayers on hydroxylated surfaces (e.g., ITO, Si, and quartz) via self-limited anaerobic chemisorption.[40,53] Molecular surface coverages, determined from cyclic voltammetry measurements, verify monolayer formation: 4.5×10^{-10} (TAA-Si_1), 4.2×10^{-10} (TAA-Si_3), 2.5×10^{-10} (TPD-Si_2), and 2.1×10^{-10} mol/cm^2 (TPD-Si_4) (data are compiled in Table 2.)[54] As a comparison, a close-packed monolayer of ferrocene dicarboxylic acid absorbed on ITO yields 4.0×10^{-10} mol/cm^2 surface coverage.[8,55] Thus, the surface coverages of trichlorosilyl-derived absorbates are similar to or less than those of the ferrocene monolayer, supporting monolayer formation in the above chemisorption process.

Two-electron redox processes are assumed in the above estimation of surface coverage for TPD-Si_2 and TPD-Si_4,[56] on the basis of the solution electrochemistry of analogous triarylamines in which multiple amino functionalities in tetraarylbenzidines analogous to TPD-Si_2 and TPD-Si_4 undergo either stepwise or simultaneous oxidation, forming cation radicals.[57] Presumably, two-electron redox processes occur in an essentially single step for TPD-Si_2 and TPD-Si_4 strongly absorbed on electrodes, suggested by cyclic voltammetry features that do not exhibit two well-resolved, consecutive one-electron redox waves (Figure 2).[58] To confirm these assumptions, we also calculated absorbate surface coverages from the electron-density profiles obtained in the XRR measurements (Table 2). It can be seen that the XRR-derived molecular footprint surface coverages are in reasonable agreement with those obtained from cyclic voltammetry measurements if two-electron processes are reasonably assumed in the cyclic voltammetric assay of the TPD-Si_2 and TPD-Si_4 films.

The self-assembled siloxane film thicknesses were also characterized by XRR, and the results were compared to molecular lengths estimated from molecular modeling. The AM1 semiempirical quantum mechanical energy-minimized structure of a bidentate hydrolyzed form of TAA-Si_3, with two of the three siloxane functionalities fixed on an imaginary plane, yields a molecular height of ~1.6 nm by measuring the distance from one oxygen atom of the unbound siloxane group to the plane. Comparing this estimated molecular height to the experimental layer thickness of 1.10 ± 0.01 nm leads to the argument that TAA-Si_3 monolayer formation occurs on average with the molecular planes

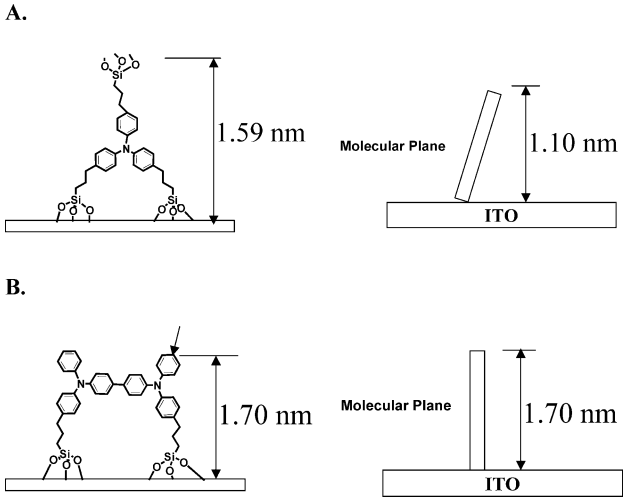

Figure 7. (a) TAA-Si_3 molecules self-assemble onto ITO substrates largely with two silyl tethers. The semiempirical AM1 energy-minimized structure of hydrolyzed TAA-Si_3 has a molecular height of 1.59 nm. (b) TPD-Si_2 molecules self-assemble onto ITO substrates largely with two silyl tethers. The semiempirical AM1 energy-minimized structure of hydrolyzed TPD-Si_2 has a molecular height of 1.70 nm.

predominantly oriented approximately perpendicular, but slightly tilted, with respect to the plane of the substrate (Figure 7a). Similarly, molecular geometry modeling of a bidentate hydrolyzed form of TPD-Si_2, with two siloxane functionalities fixed on an imaginary plane, yields an estimated molecular height of ~1.7 nm by measuring the distance from the carbon atom (labeled in Figure 7b) to the plane. This is in excellent agreement with the XRR-measured film thickness (1.78 ± 0.01 nm), indicating that TPD-Si_2 monolayer formation occurs with the molecular planes predominantly oriented in the direction normal to the substrate surface. Similar modeling of monodentate TAA-Si_1 and bidentate TPD-Si_4 yields molecular heights of 1.6 nm (TAA-Si_1) and 1.7 nm (TPD-Si_4), which are again in favorable agreement with the XRR-derived thicknesses, assuming some tilting in the former absorbate (Table 2). Thus, it is argued that the various trichlorosilyl-tethered probe molecules undergo self-assembly on the hydroxylated surface, driven by siloxane condensation, to form relatively dense and pinhole-free monolayers. The chemisorptive reactions halt at the point that negligible surface hydroxyl functionalities are accessible for further condensation with the silyl tethers.[40,53]

Probing ITO Anode−HTL Interfacial Molecular Structure Effects Using the Self-Assembled Siloxane Films. To address the problem stated at the outset, we developed a molecular probe approach here to study the effects of anode−HTL interfacial molecular structure on OLED response. The following probe design criteria are fulfilled so that the effects of probe molecular structure on hole injection across the ITO anode−HLT interface and subsequent OLED response can be analyzed: (1) Probe must be precisely deliverable in the nanoscale interfacial region. As discussed above, the probe molecules form less than 2 nm thick conformal, strongly bound, electroactive, largely pinhole-free films on the ITO surface. Followed by deposition of a HTL, the molecules are precisely located at the ITO anode−HTL interface, which is defined as the <5 nm thick region proximate to the ITO

(53) Silberzan, P.; Leger, L.; Ausserre, D.; Benattar, J. J. *Langmuir* **1991**, *7*, 1647−51.
(54) Murray, R. W. In *Molecular Design of Electrode Surfaces, Techniques of Chemistry*; Murray, R. W., Ed.; Wiley: New York, 1992; Vol. 22, pp 1−158.
(55) Zotti, G.; Schiavon, G.; Zecchin, S.; Berlin, A.; Pagani, G. *Langmuir* **1998**, *14*, 1728−1733.
(56) Zhuang, B.; McDonald, J.; Schultz, F.; Newton, W. *Organometallics* **1984**, *3*.
(57) Faber, R.; Mielke, G. F.; Rapta, P.; Stasko, A.; Nuyken, O. *Collect. Czech. Chem. Commun.* **2000**, *65*, 1403−1418.
(58) Rosenhein, L.; Newton, W.; McDonald, J. *Inorg. Chem.* **1987**, *26*, 1695−1702.

surface.[11] This ensures only interfacial phenomena are probed by the molecules, without interference of bulk effects. (2) The probe must be hole-transport active. UPS measurements reveal that the triarylamine siloxane thin films have IP potentials and HOMO energy levels favorable for hole injection (Scheme 4). Furthermore, cyclic voltammetry indicates that the probe molecules are capable of transporting holes when chemisorbed on the ITO surface. (3) The probes need systematically adjustable molecular structures. The incrementally varied trichlorosilylpropyl tether numbers (1−4) combined with variable numbers of triarylamine units (1 or 2) in the probe molecular structures result in varied SAM structures and, consequently, varied hole fluence and OLED response, as discussed below.

SAM Structural Variation Induced by Systematically Adjusted Probe Molecular Structures. It is expected that SAMs fabricated with architecturally different probe molecules will have differing film microstructures. Indeed, this is observed in the thin-film characterization data presented here. First, different types of probe molecule triarylamine cores profoundly affect SAM structure, as indicated by different voltammetry behavior (e.g., $E_{p,a}$ and $E_{p,c}$, Table 1). Similarly, the core structures are known to exhibit different formal oxidation potentials in solution (E^0 (V vs SCE) = 0.72, 0.96 (TPD); 1.02 (TAA)).[57] Second, the SAMs have differing intermolecular interactions between triarylamine cores, likely arising from the differing probe molecular shapes and linker densities. Cyclic voltammetry of the SAMs on ITO electrodes at room temperature reveals that the full width at half-height of the oxidative wave ($\Delta E_{p,1/2}$) at the slowest sweep rate (0.1 V/s) is 340 (TAA-Si_1), 350 (TPD-Si_2), 440 (TPD-Si_4), and 460 mV (TAA-Si_3). For ideal Nernstian electrochemical reactions of identical, independent anchored redox site ensembles at room temperature, $\Delta E_{p,1/2}$ of either of the symmetrically disposed cathodic or anodic peaks is expressed as in eq 2[59]

$$\Delta E_{p,1/2} = 90.6/n \text{ mV} \quad (2)$$

Deviation from this ideal behavior, seen as broadening or distortion of the electrochemical waves, often indicates redox site−site interactions and/or site heterogeneity.[45,46,60] The symmetrical voltammetry characteristics seen in Figure 2 at a slow sweep rate indicate that the electron transfer between immobilized triarylamine cores and the electrode is rapid and reversible on the time scale of the experiment.[45] Quantitatively, the value of $\Delta E_{p,1/2}$ is related to $g = \alpha_o + \alpha_R - 2\alpha_{OR}$, where α_o, α_R, and α_{OR} are the interaction parameters for oxidative site−oxidative site, reductive site−reductive site, and oxidative site−reductive site interactions, with $\alpha > 0$ for attractive interactions and $\alpha < 0$ for repulsive ones. When $g = 0$, $\Delta E_{p,1/2} = 90.6/n$; when $g < 0$, $\Delta E_{p,1/2} > 90.6/n$. Qualitatively, stronger redox site interactions result in larger deviations of $\Delta E_{p,1/2}$ from the ideal value.[61,62] Presumably, then, the intermolecular interactions in the present SAMs follow this order of $\Delta E_{p,1/2}$ values: TAA-Si_3 > TPD-Si_4 > TPD-Si_2 > TAA-Si_1. SAM-modified ITO anode−NPB HTL interfaces thereby have different nanoscale intermolecular interactions, affecting interfacial charge injection/transport.[14,15] Further comments about rates of heterogeneous electron transfer are made below.

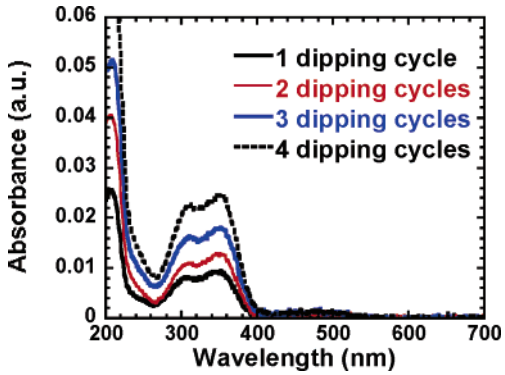

Figure 8. UV−vis absorption spectroscopic monitoring of TPD-Si_4 self-assembly on quartz substrates.

Additionally, it is possible that the distance from the triarylamine cores to the ITO surface varies as a function of the probe molecule geometry and linker density. TAA-Si_3 and TPD-Si_4 have three or four silyl linkers, respectively, whereas TAA-Si_1 and TPD-Si_2 have one or two, respectively. In principle, the former two should lie predominantly flat on the ITO surface, minimizing the triarylamine−anode distance, whereas the latter two should stand up, leading to different charge-injection/-transport characteristics.[63] The XRR-derived SAM thickness/roughness data combined with molecular modeling show that TAA-Si_3 in fact anchors largely via one or two linkers rather than three, similar to situations seen previously,[64] whereas TPD-Si_4 apparently adopts both flat and upright orientations, yielding an unusually rough SAM surface (Table 2). The roughness:thickness ratio is 0.80 (TPD-Si_4) vs 0.44 (TPD-Si_2), 0.36 (TAA-Si_1), and 0.55 (TAA-Si_3). To further support these arguments, we carried out successive layer-by-layer deposition of TPD-Si_4 SAMs on quartz substrates and measured optical absorption spectra after each step in the dipping process (Figure 8). If TPD-Si_4 utilizes all four trichlorosilyl tethers in the self-assembly, single-monolayer coverage should be favored, as observed in the deposition of TPD-Si_2.[20] On the contrary, multilayer coverages are achieved in the layer-by-layer deposition of TPD-Si_4, resulting in increased optical absorption with additional dipping cycles (unlike with TPD-Si_2). Thus, the TPD-Si_4 SAM can undergo self-assembly on ITO surfaces in either a flat or upright orientation, with unreacted silanol groups available for hydrolysis and subsequent linkage to new layers. Furthermore, chemisorbed TPD-Si_4 should have a smaller triarylamine core−ITO anode spacing compared to the other three SAMs because of the four-tether-linked configuration not possible in other SAMs studied here.

Large Variations in Hole-Injection Efficiency and OLED Response Effected by Different SAMs. Precisely

(59) Bard, A. J.; Faulkner, L. A. *Electrochemical Methods—Fundamentals and Applications*; Wiley: New York, 1984; pp 580−631.
(60) Clark, R. A.; Bowden, E. F. *Langmuir* **1997**, *13*, 559−565.
(61) Zhang, W. W.; Ren, X. M.; Li, H. F.; Lu, C. S.; Hu, C. J.; Zhu, H. Z.; Meng, Q. J. *J. Colloid Interface Sci.* **2002**, *255*, 150−157.
(62) Nielsen, M.; Larsen, N. B.; Gothelf, K. V. *Langmuir* **2002**, *18*, 2795−2799.
(63) Smalley, J. F.; Feldberg, S. W.; Chidsey, C. E. D.; Linford, M. R.; Newton, M. D.; Liu, Y. P. *J. Phys. Chem.* **1995**, *99*, 13141−13149.
(64) Li, Z. Y.; Lieberman, M.; Hill, W. *Langmuir* **2001**, *17*, 4887−4894.

located at the ITO anode−HTL interface, the triarylamine siloxane SAMs result in large variations in hole-injection efficiency and OLED response, as seen in Figures 4−6. Interestingly, the large variations cannot be explained solely on the basis of current models of ITO anode modification effects on hole-injection efficiency.[16,28−35] Any interfacial dipole moment effects would appear to be relatively small, as indicated by the ±0.1 eV of vacuum level shift induced by TPD-Si_2 SAMs in UPS measurements, and cannot be fully responsible for the dramatic hole injection and EL response enhancements evident in Figures 4−6. The SAMs have similar 1−2 nm thicknesses and, consequently, should have similar image force effects on injected charges.[25] As seen in Scheme 4, the SAMs have similar HOMO and LUMO energy levels, and thus should decrease the anode−HTL HOMO energetic barrier and confine electrons to emissive layers similarly. Surface-energy-promoted wetting/cohesion at the ITO−organic layer interface, a significant factor in hole-injection efficiency, as demonstrated in our previous work,[20,34,65] cannot fully explain the large hole-injection variations effected by the SAMs. All four SAMs should similarly attenuate the ITO anode−HTL interfacial surface energy mismatch, as qualitatively indicated by the increased advancing aqueous contact angles of the SAM-coated ITO surfaces vs that of bare ITO substrates. However, there is no measurable difference between the SAM contact angles, rendering any correlation between contact-angle-indexed surface energy and hole-injection efficiency inconclusive. To further investigate this point, we also deposited phenyltrichlorosilane onto ITO surfaces following the same procedure as that for the SAM deposition. The resulting coated ITO substrates exhibit advancing aqueous contact angles (80−86°) close to those of the triarylamine SAMs. The OLED response of devices with the structure ITO/phenylsiloxane/NPB/Alq:1% DIQA/Al was measured and is reported in Figure 9, together with that of ITO/SAM/NPB/Alq:1% DIQA/Al. It can be seen that the former displays significantly poorer device response (maximum light output = 6800 cd/m^2, maximum forward external quantum efficiency = 0.39%). This is also true for OLEDs with the structure ITO/phenylsiloxane/NPB/Alq:1% DIQA/BCP/Li/AgMg vs ITO/SAM/NPB/Alq:1% DIQA/BCP/Li/AgMg (Figure 10). These results support the above argument that the modified surface energy of the ITO surface is not the sole origin of the observed OLED response enhancements. Other factors at the ITO anode−HTL interface to be considered for explaining the SAM-associated interfacial phenomena are discussed below.

Correlation between SAM Structural Variations and Hole-Injection Efficiency and OLED Response. SAM structural variations arising from the different probe molecular structures are clearly evident in the various thin-film characterizations, as discussed above. Furthermore, the large variation in hole-injection efficiency and OLED response seen in Figures 4−6 can be correlated with the SAM structural variations. Note that the SAMs are covalently grafted onto the ITO surface, contain redox-active triarylamine moieties, and undergo numerous solid-state oxidation−reduction cycles during OLED operation.[66] A priori, it might therefore be hypothesized, although never previously verified, that electrochemical heterogeneous electron-transfer rates between the ITO electrode and the SAM redox sites are related to the charge-injection/-transport efficiency across the SAMs in operating OLEDs. Indeed, such a correlation is observed here for the first time. Cyclic voltammetry of the SAMs on ITO electrodes (scan rate = 10 V/s) reveals E_{ox}/E_{red} peak separations increasing in the order 331 mV (TPD-Si_4) < 345 mV (TPD-Si_2) < 382 mV (TAA-Si_1) < 466 mV (TAA-Si_3). Such data can be used to estimate interfacial electron-transfer rates for strongly absorbed redox-active sites.[44,67,68] In general, the observed peak potential separation depends on the relative scan rates and electron-transfer rates. All other factors being equal, larger peak separations qualitatively correlate with slower interfacial electron transfer.[44,46,67,69] As demonstrated here, this electrochemical index of heterogeneous charge-injection/-

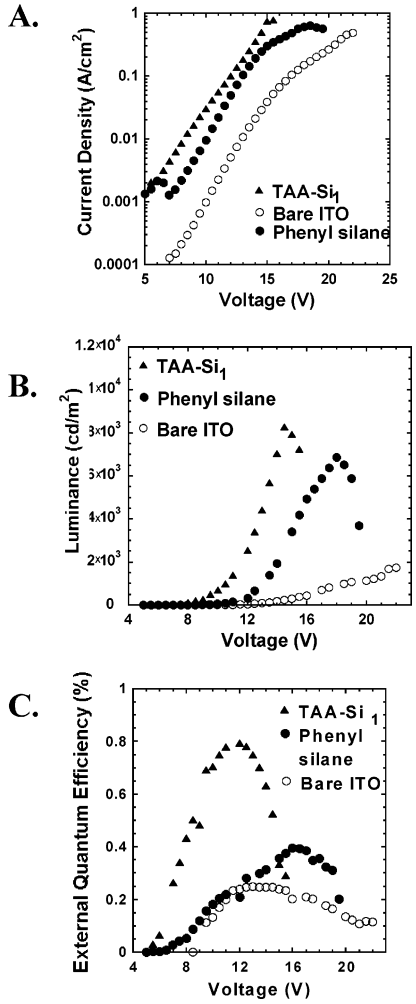

Figure 9. Responses of OLEDs with structures ITO/phenylsiloxane SAM/NPB/Alq:1% DIQA/Al. (a) Current density vs voltage; (b) luminance vs voltage; (c) external forward quantum efficiency vs voltage.

(65) Cui, J.; Huang, Q.; Wang, Q.; Marks, T. J. *Langmuir* **2001**, *17*, 2051−2054.

(66) Aziz, H.; Popovic, Z. D. *Appl. Phys. Lett.* **2002**, *80*, 2180−2182.
(67) Finklea, H. O.; Liu, L.; Ravenscroft, M. S.; Punturi, S. *J. Phys. Chem.* **1996**, *100*, 18852−18858.
(68) Laviron, E. *J. Electroanal. Chem.* **1979**, *101*, 19−28.
(69) Finklea, H. O.; Hanshew, D. D. *J. Am. Chem. Soc.* **1992**, *114*, 3173−3181.

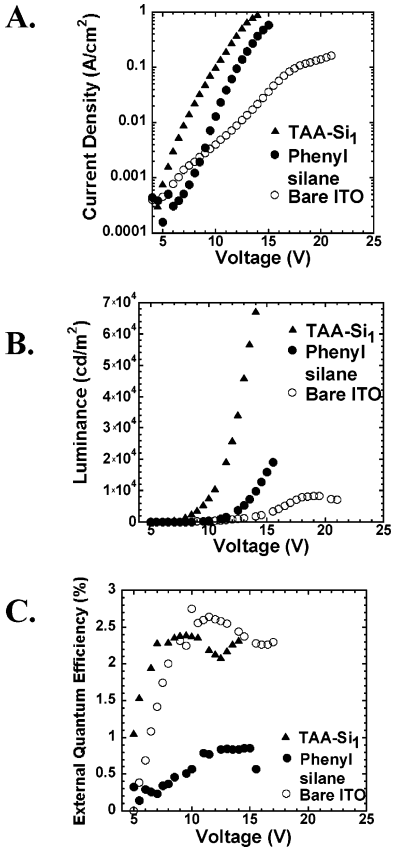

Figure 10. Responses of OLEDs with structures ITO/phenylsiloxane SAM/NPB/Alq:1% DIQA/BCP:Li/AgMg. (a) Current density vs voltage; (b) luminance vs voltage; (c) external forward quantum efficiency vs voltage.

transport efficiency correlates closely with the solid-state hole-only device injection/transport capacity: TPD-Si_4 > TPD-Si_2 > TAA-Si_1 > TAA-Si_3 (Figure 4).

The above correlation between the electrochemical electron-transfer rates and charge injection across the SAMs at the ITO anode−electrolyte or organic solid interface argues that knowledge of how the compositions and structures of redox-couple-containing thin films absorbed on electrode surfaces impact electron transfer between the electrode and the redox sites in an electrochemical system can be applied to understanding large variations in hole-injection efficiency and OLED response with SAM structure.[43,54,59] More specifically, the SAM structures vary in triarylamine cores with different E^0 values,[57] distances from the triarylamine cores to the ITO surface,[63] differing intermolecular interactions between neighboring triarylamine cores,[45,46,61,62,67] and SAM reorganization energies.[54,70] The effects of these structural variations on OLED hole injection and response can be understood on the basis of their effects on the electrochemical heterogeneous electron transfer in ways that are well documented.

Generally, electron transfer between a redox couple and an electrode is described via a superexchange interaction[71] where electronic coupling is dominated by through-bond electron tunneling.[72] However, through-space nonbonded contacts also contribute to the electrode−redox couple electronic coupling, especially when the redox potentials of linkers and redox couples are very different.[73−76] In the SAMs studied here, the triarylamine core redox couples are covalently linked to the ITO electrode via alkyl chains having the same length, so the through-bond electron tunneling probability between the electrode and the redox couple is likely to be similar for all of the present SAMs.[72] Nevertheless, the redox couple is spatially more proximate to the electrode in the case of TPD-Si_4, as discussed earlier; the through-space electronic coupling should be stronger, resulting in more-rapid electron transfer, as confirmed in the cyclic voltammetry measurements, and a greater charge-transport capacity, as seen in hole-only devices.[77]

The effect of intermolecular interactions on electron-transfer involving SAMs is also often observed in electrochemical studies[59,60] and is attributable to intermolecular electronic coupling, which also affects the electron-transfer rates.[67,72] It is reasonable to argue that the different intermolecular interactions observed between triarylamine cores in the present SAMs play a significant role in the varied electrochemical electron-transfer rates and OLED hole-injection patterns. In addition, the different SAMs may have different reorganization energies, which should also affect electrochemical electron-transfer rates, as described by Marcus theory.[78,79] In the scenario of surface-confined redox couples, the electron-transfer rate between the redox species and an electrode can be described in a simplified form (eq 3)[46,70,80,81]

$$k_{et} = \exp[-(\lambda + \Delta G^0)^2/4\lambda RT] \quad (3)$$

where λ is the reorganization free energy and ΔG^0 is the reaction free energy equal to $e(E - E^0)$ (e is the electron charge, E is the electrode potential, and E^0 is the formal potential of the redox couple[81]). Similar effects should be important for charge injection across SAMs in OLED configurations.

Conclusions

A series of silyltriarylamine molecules are designed, synthesized, and self-assembled onto ITO anode surfaces, forming nanometer-scale thin films. Their large effects on OLED hole-injection and EL properties correlate with electrochemical heterogeneous electron-transfer characteristics and OLED anode−organic interfacial molecular structures in a way that has not been previously observed in other OLED interfacial phenomenon studies. Chemically tuning

(70) Newton, M. D.; Sutin, N. *Annu. Rev. Phys. Chem.* **1984**, *35*, 437.
(71) Newton, M. D. *Chem. Rev.* **1991**, *91*, 767−792.
(72) Napper, A. M.; Liu, H. Y.; Waldeck, D. H. *J. Phys. Chem. B* **2001**, *105*, 7699−7707.
(73) Napper, A. M.; Read, I.; Waldeck, D. H.; Head, N. J.; Oliver, A. M.; Paddon-Row, M. N. *J. Am. Chem. Soc.* **2000**, *122*, 5220.
(74) Kumar, K.; Lin, Z.; Waldeck, D. H.; Zimmit, M. B. *J. Am. Chem. Soc.* **1996**, *118*, 243.
(75) Yamamoto, H.; Waldeck, D. H. *J. Phys. Chem. B* **2002**, *106*, 7469.
(76) Forster, R. J. *Inorg. Chem.* **1996**, *35*, 3394−3403.
(77) In principle, SAM π-system overlap with ITO band structure may be important. However, there is insufficient structural information to confirm this.
(78) Marcus, R. A. *J. Phys. Chem.* **1963**, *67*, 853.
(79) Marcus, R. A. *Angew. Chem., Int. Ed.* **1993**, *32*, 1111.
(80) Nahir, T. M.; Clark, R. A.; Bowden, E. F. *Anal. Chem.* **1994**, *66*, 2595−2598.
(81) Chidsey, C. E. *Science* **1991**, *251*, 919.

the interface structure represents an effective approach for studying nanoscale injection layers and yields Alq-based OLEDs with high brightness (~70 000 cd/m^2), low turn-on voltages (~4 V), and high efficiencies (2.5% external forward quantum efficiency).

Acknowledgment. We thank the NASA Institute for Nanoelectronics and Computing (NCC2-3163) and the NSF-MRSEC program through the Northwestern Materials Research Center (DMR-0076097) for support of this research. We thank Prof. N. Armstrong and Dr. P. Lee (University of Arizona) for UPS measurements, and Drs. G. Hutchison, B. Scott, and J. Veinot for helpful discussions.

Supporting Information Available: Synthesis and characterization of interfacial modification precursors TPD-Si_4 and TAA-Si_1; UV−vis absorption spectra, AFM images, and XRR data of SAMs of TAA-Si_1, TAA-Si_3, TPD-Si_2, and TPD-Si_4; table of self-assembled siloxane-film-characterization data including advancing aqueous contact angles. This material is available free of charge via the Internet at http://pubs.acs.org.

CM0604918